Mon. Not. R. Astron. Soc. **000**, 1–9 () Printed 21 February 2015 (MN LaTeX style file v2.2)

Tumbling asteroid rotation with the YORP torque and inelastic energy dissipation

S. Breiter[1]⋆ and M. Murawiecka[1]†
[1]*Astronomical Observatory Institute, Faculty of Physics, Adam Mickiewicz University, Sloneczna 36, PL60-286 Poznań, Poland*

ABSTRACT

The Yarkovsky-O'Keefe-Radzievskii-Paddack (YORP) effect and rotational energy dissipation due to inelastic deformations are two key mechanisms affecting rotation of tumbling asteroids in long term. Each of the effects used to be discussed separately. We present the first results concerning a simulation of their joint action. Asteroids (3103) Eger and (99942) Apophis, as well as their scaled variants, are used as test bodies. Plugging in the dissipation destroys limit cycles of the pure YORP, but creates a new asymptotic state of stationary tumbling with a fixed rotation period. The present model does not contradict finding Eger in the principal axis rotation. For Apophis, the model suggests that its current rotation state should be relatively young. In general, the fraction of initial conditions leading to the principal axis rotation is too small, compared to the actual data. The model requires a stronger energy dissipation and weaker YORP components in the nutation angle and obliquity.

Key words: celestial mechanics—minor planets, asteroids: general—minor planets, asteroids: individual: (3103) Eger, (99942) Apophis

1 INTRODUCTION

The radiation torques, usually referred to as the YORP (Yarkovsky-O'Keefe-Radzievskii-Paddack) effect, have been shown to dominate the secular evolution of spin state of small Solar System bodies. Since the first notion by Rubincam (2000), several features of this effect have been examined. In particular, the strength of YORP has been proven to depend strongly on the shape of the body, including also medium and minor scale surface features (Statler 2009; Breiter et al. 2009). The induced changes in obliquity depend strongly on the assumed value of thermal conductivity (Čapek & Vokrouhlický 2004). The role of conductivity in the rotation rate evolution depends on the adopted model: it comes into play mostly through the conduction in small boulders, as shown by Golubov & Krugly (2012).

The vast majority of earlier works dealt with the YORP effect under a simplifying assumption of principal axis rotation, in which the body spins around the axis of maximum inertia. Corresponding to the minimum of kinetic energy, this state has often been heuristically argued to be a reasonable assumption. Only a few papers considered the problem of the YORP effect in general rotation state. The numerical simulation of Vokrouhlický et al. (2007) discovered asymptotic tumbling states with constant obliquity of angular momentum, but involving secular variations of the rotation period. Cicaló & Scheeres (2010) issued a semi-analytical model that occurred to be conservative, but suggested that a further development may lead to the asymptotic nature of the newly found equilibria. Finally, Breiter, Rożek & Vokrouhlický (2011) pushed the semi-analytical model further and not only obtained the agreement with Vokrouhlický et al. (2007), but also discovered a new type of asymptotic states – limit cycles.

The YORP effect is not the only nongravitational factor to be taken into account when the non-principal axis (NPA) rotation of small bodies is considered. Another important mechanism acts due to periodically oscillating centrifugal acceleration of NPA. The body responds by periodic deformations, with a fraction of mechanical energy lost as heat in each stress-strain cycle. Conserving the total angular momentum, the mechanism drains kinetic energy, which leads to the nutation damping – the spin axis drifts towards the principal axis of maximum inertia, leaving the rotation rate intact. The more excited wobbling is, the more intensively the energy is dissipated. This mechanism, identified by Prendergast (1958), has been thoroughly studied within a standard quality factor approximation (e.g. Burns & Safronov 1973; Efroimsky 2000; Sharma et al. 2005; Breiter et al. 2012), but none of existing solutions is considered entirely satisfactory. In particular, using the quality factor Q as a constant parameter, independent on the forcing frequency, has met a harsh criticism (e.g. Efroimsky & Makarov 2013). Nevertheless, there exist generic properties of the inelastic dissipation process in asteroids. For example, a faster spinning object should damp the nutation more efficiently than a similar object spinning slower. On the other hand, the rule that larger bodies damp nutation faster hinges upon the (arguable) assumption of size-independent quality factor Q.

⋆ E-mail:breiter@amu.edu.pl
† E-mail:magda.murawiecka@gmail.com

Recently, Wiegert (2015) reminded about meteoroid impacts as another important factor, but this effect will be left beyond the scope of the present analysis.

The majority of asteroids are found in the principal axis rotation; up to date, only 58 objects have been identified as the NPA rotators (Pravec et al. 2014). In principle, it means that the inelastic energy dissipation dominates over such tumbling triggers as collisions, close flybys, and the YORP effect. However, the problem also has an observational selection aspect: tumbling objects are a significant fraction of smaller asteroids with a long rotation period – both properties unfavorable for photometry (Pravec et al. 2014).

The present work is the first attempt to see the combined action of the YORP and inelastic nutation damping models. To this end, we integrated the averaged equations of rotation adding the right hand sides taken from two papers by Breiter, Rożek and Vokrouhlický (2011; 2012). The former is a semi-analytical description of spin-state evolution of an asteroid under the action of the YORP torque, whereas the latter presents an analytical solution for energy dissipation in the case of a freely rotating triaxial ellipsoid.

Section 2 briefly describes our semi-analytical model and the general form of the equations to be integrated. Only the most essential information is given, but an interested reader may find missing details in the two referenced articles. Section 3 provides data for two sample asteroids to be analyzed: (3103) Eger and (99942) Apophis. The choice is rather arbitrary, but not random. The case of YORP on a tumbling Eger-shaped object was studied in the earlier paper, which allows a comparison of the new results with numerous figures from Breiter et al. (2011). The recent observations of Apophis found it in a well determined tumbling state and the influence of inelastic dissipation (without YORP) is discussed in Pravec et al. (2014). Thus, we choose one non-tumbler with YORP discussed earlier, and one actual tumbler with published nutation damping considerations, and ask about the change in picture after treating the joint YORP and dissipation mechanism. The results for both objects, as well as for their scaled versions, are presented in Section 4. In Section 5 we try to establish fractions of possible final states on a grid of initial conditions. General conclusions are stated in Section 6.

2 MODEL

In order to follow the concurrent action of radiation torques and inelastic dissipation on an asteroid within a reasonable computation time, one should use equations of motion averaged at least with respect to rotation angle, but preferably with respect to the precession and nutation angles, and orbital motion as well. With this requirement, striving for best semi-analytical models available, the authors had a very limited choice.

Most of the dissipation models refer to spheroid – an unrealistic model for irregular minor bodies. The notable exception of a triaxial cuboid considered by Efroimsky (2000) was restricted to small deviations of angular momentum vector from the principal axis. The only alternative has been to use the results of Breiter et al. (2012), providing the energy dissipation formula for a homogeneous triaxial ellipsoid.

As far as the YORP effect is concerned, the only two models allowing a tumbling rotation are these of Cicaló & Scheeres (2010) and Breiter et al. (2011). As mentioned in the Introduction, the former is not realistic because of a prematurely truncated expansion of the insolation function, hence the choice of the latter, in spite of all its shortcomings. Its notable limitations include, first of all, the absence of heat conduction effects. Others, which might be overcome in future, but have been adopted in the present work, involve the homogenous, convex shape model and Lambertian scattering and emission.

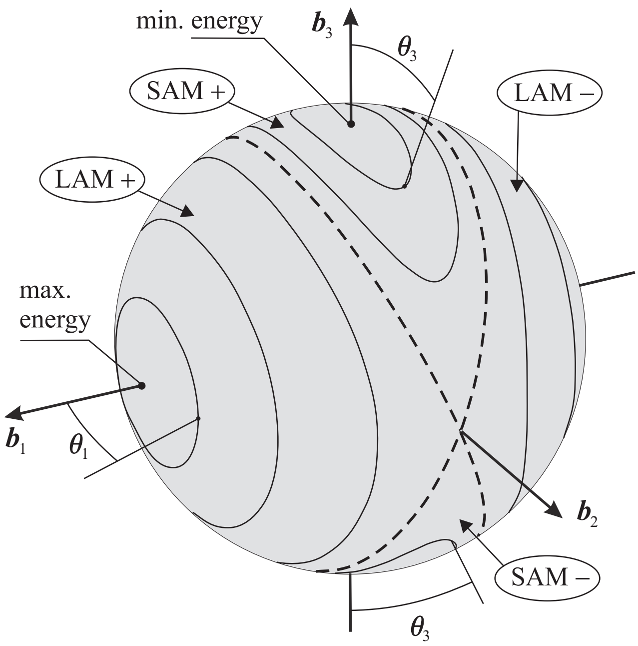

Figure 1. Angular momentum vector $\boldsymbol{G}$ evolution on a G = const sphere in the body frame $\boldsymbol{b}_1, \boldsymbol{b}_2, \boldsymbol{b}_3$ for the free rotation of Eger. Dashed lines mark the separatrices as borderlines between four rotation modes. Nutation angle θ_s for three exemplary rotation curves is shown.

In present work, we consider two types of excited rotation: short-axis (SAM) and long-axis (LAM) modes, depending on which principal axis of inertia the angular momentum vector $\boldsymbol{G}$ circulates around. Moreover, setting a body frame with axes $\hat{\boldsymbol{b}}_1$, $\hat{\boldsymbol{b}}_2$, $\hat{\boldsymbol{b}}_3$, with $\hat{\boldsymbol{b}}_1$ along the minimal and $\hat{\boldsymbol{b}}_3$ the maximal axis of inertia tensor, we discriminate between SAM+ and SAM–, according to the sign of the product $\hat{\boldsymbol{G}} \cdot \hat{\boldsymbol{b}}_3$; similarly, we speak about LAM+ or LAM– according to the sign of $\hat{\boldsymbol{G}} \cdot \hat{\boldsymbol{b}}_1$ in the LAM case (see Fig. 1). In order to reduce the number of variables, we use the angular momentum length $G = \| \boldsymbol{G} \|$ and two polar angles: obliquity ε between orbital angular momentum (normal to the orbit plane) and $\boldsymbol{G}$, and the nutation angle θ – understood as the maximum value of angle between $\boldsymbol{G}$ and a relevant principal axis $\boldsymbol{b}_3$ or $\boldsymbol{b}_1$ attained during one nutation cycle (see Fig. 1). The latter is closely related to the dynamical inertia $\Delta = \mathcal{A}^{-1}$ from Breiter et al. (2011) and replaced it in Breiter et al. (2012).

Even if the body frame for a particular object is right-handed, and aligned with the principal axes of the inertia ellipsoid, the particular choice of $\boldsymbol{b}_i$ direction remains arbitrary (i.e. arbitrarily fixed by the authors of the shape model). The influence of reflection $\boldsymbol{b}_i \to -\boldsymbol{b}_i$ on two physical components of our model is different. The energy dissipation, based upon a symmetric ellipsoid model, is simply invariant with respect to reflection. For the action YORP, one should bear in mind the fact that it results from the net torque of an asymmetric body surface, hence it inherits the properties of vector product. A simple reflection $\boldsymbol{b}_i \to -\boldsymbol{b}_i$ changes the handedness of the frame, leading to the inversion of the torque direction. This explains why the YORP components of evolution in

SAM+ and SAM– (or LAM+ and LAM–) differ only by the direction of the flow. On the other hand, combining two reflections, like $(\boldsymbol{b}_1, \boldsymbol{b}_3) \to (-\boldsymbol{b}_1, -\boldsymbol{b}_3)$, equivalent to a rotation, simply results in the new SAM+ looking like the previous SAM– etc. Anyway, although the particular location of SAM+/– or LAM+/– is a matter of axes choice, the two regimes have to be distinguished in all studies involving the YORP effect.

Adding the right hand sides of the averaged equations of motion from Breiter et al. (2011) and Breiter et al. (2012) we obtain the following set for the mean angular momentum, obliquity and nutation angle with the subscript s referring to the mode ($s = 1$ for LAM and $s = 3$ for SAM)

$$\dot{G}_s = -\frac{\kappa'}{\mathrm{K}(k_s)} \sum_{n \geqslant 1} \Theta^0_{2n}(\cos\varepsilon)\, G_{s,n}, \tag{1}$$

$$\dot{\varepsilon}_s = -\frac{\kappa'}{G_s\,\mathrm{K}(k_s)} \sum_{n \geqslant 1} \Theta^1_{2n}(\cos\varepsilon)\, E_{s,n}, \tag{2}$$

$$\begin{aligned} \dot{\theta}_s = {} & \frac{a^4 \rho m G_s^3 a_s^5}{\mu Q (a_s - a_2)} \frac{\Psi_s}{\sin\theta_s \cos\theta_s} \\ & + \frac{\kappa'}{G_s\,\mathrm{K}(k_s)} \frac{a_2 - (a_2 - a_s)\cos^2\theta_s}{(a_2 - a_s)\sin\theta_s\cos\theta_s} \sum_{n \geqslant 1} \Theta^0_{2n}(\cos\varepsilon)\, \Delta_{s,n}. \end{aligned} \tag{3}$$

Explaining the multitude of symbols present in the above equations, let us begin with the YORP related $G_{s,n}$, $E_{s,n}$, $\Delta_{s,n}$, which are functions depending on the shape of the body and current θ_s angle value; their explicit form is rather extensive and can be found in Breiter et al. (2011). Θ^m_{2n} are normalized associated Legendre functions (of degree $2n$ and order m). $\mathrm{K}(k_s)$ stands for the complete elliptic integral of the first kind; its modulus k_s depends on nutation angle (both the quoted papers use the same quantity, its expression in terms of θ_s is given in Breiter et al. (2012)). Ψ_s, depending on θ_s, is the energy dissipation function as expressed in Breiter et al. (2012). Actually, all the enumerated functions depend also on the principal moments of inertia I_j through their inverse values

$$a_j = \frac{1}{I_j}. \tag{4}$$

Physical parameters include Lamé elasticity (shear) modulus μ, quality factor Q, bulk density ρ, mass m, and the major semi-axis of the equivalent ellipsoid a used in the nutation damping term. The factor κ'

$$\kappa' = \frac{\pi}{3} \frac{V \Phi_0}{c\sqrt{1-e^2}} \left(\frac{d_0}{a_\mathrm{o}}\right)^2, \tag{5}$$

involves the velocity of light c, body volume V, orbital eccentricity e, orbital semi-axis a_o, and nominal heliocentric distance $d_0 = 1$ au for the solar constant Φ_0.

The energy dissipation does not directly affect angular momentum or obliquity, so the relevant term is added only in $\dot{\theta}_s$ equation. Still, the YORP effect depends on nutation angle, so the contribution in θ_s due to dissipation influences $\dot{G}_s$ and $\dot{\varepsilon}_s$ as well. Moreover, one can observe that increasing rotation rate reduces the strength of YORP in obliquity and nutation angle (division by G_s in the right hand sides) while boosting the energy dissipation rate.

Equations (1-3) describe the secular evolution of the system, averaged with respect to rotation, precession-nutation and orbital motion. They must be integrated numerically, which we did with the use of RA15 – 15-th order Radau-Everhart integrator (Everhart 1985). We excluded from the considerations two regions of motion: the vicinity of separatrices between SAM and LAM, where the chaotic zone arises (there the averaging process fails), and the close neighborhood of the principal axes. The latter exclusion is technical – due to an apparent singularity in the present form of the energy dissipation term. Accordingly, we set the integration limits in nutation angle to $0\overset{\circ}{.}1 < \theta_s < 85^\circ$. We also exclude the rotation so slow that it violates the averaging assumptions, assuming the rotation period of 10 years as a limit.

In the next sections we omit the subscript s for the sake of brevity, assuming that its value either follows from the context (SAM or LAM mode discussed), or is irrelevant for general considerations.

3 SAMPLE OBJECTS

For the reasons explained in Introduction, we consider two exemplary asteroids. The first one, (3103) Eger, has the volume $V \approx 0.419 \times 10^{10}$ m^3 (effective radius 1 km), and the moments of inertia equal $I_1 = 0.245 \times 10^{19}$, $I_2 = 0.518 \times 10^{19}$, $I_3 = 0.634 \times 10^{19}$ kg m^2, if density $\rho = 2000$ kg/m^3 is assumed. The torque coefficients for the convex shape model are included in Table D1 of Breiter et al. (2011). We take the observational value of rotational period $P = 5.7$ h as the starting point for the estimation of initial angular momentum.

The second object is (99942) Apophis, which has been recently found to be in a tumbling spin state by Pravec et al. (2014). Photometric data imply that this asteroid exhibits SAM rotation with $\theta = 55^{\circ}{}^{+9}_{-20}$ and period $P = 30.56$ h. The rotation is retrograde, because the angular momentum vector is tilted in respect to the orbit normal with the obliquity $\varepsilon = 165^\circ$. According to the newest observational data quoted by Müller et al. (2014), the volume of this object is $V \approx 2.76 \times 10^7$ m^3 (effective radius 187 m), leading to the moments of inertia $I_1 = 0.296 \times 10^{15}$, $I_2 = 0.475 \times 10^{15}$, $I_3 = 0.513 \times 10^{15}$ kg m^2, in the convex shape model of Pravec et al. (2014). The leading YORP torque coefficients, computed according to this shape, are gathered in Tab. 1. Similarly to Eger, we assume $\rho = 2000$ kg/m^3.

Figure 1 has been plotted using the moments of inertia of Eger. With these values, the area of SAM is significantly smaller than the one of LAM. Actually, the case of Apophis has the same property.

In order to apply the energy dissipation model of Breiter et al. (2012), the equivalent ellipsoid semi-axes are necessary. They can be determined in terms of the actual principal moments of inertia tensor of an asteroid. For the semi-axes $c < b < a$, the appropriate expressions are

$$c = \sqrt{\frac{5\,(I_1 + I_2 - I_3)}{2m}}, \tag{6}$$

$$b = \sqrt{\frac{5\,I_1}{m} - c^2}, \tag{7}$$

$$a = \sqrt{\frac{5\,I_2}{m} - c^2}. \tag{8}$$

In all computations we use the usual value of the damping factor $\mu Q = 10^{11}$ Pa (e.g. Pravec et al. 2014).

4 RESULTS

4.1 (3103) Eger

First, let us recall the YORP-only evolution of an Eger-shaped object. Breiter et al. (2011) recorded some equilibria points in nutation and obliquity angles with unlimited growth or decrese of angu-

Table 1. YORP torque coefficients of (99942) Apophis for the model of Breiter et al. (2011).

n	m	$x_{n,m}$	$y_{n,m}$	$z_{n,m}$
2	0	−0.00798098	0.0	0.00159986
2	1	0.0011569	−0.000149372	−0.00599647
2	2	−0.00266466	0.00659003	0.0129006
4	0	0.000331171	0.0	−0.00136936
4	1	−0.000231354	0.0013934	−0.000936665
4	2	−0.0000532971	0.000271434	−0.00084783
4	3	−0.000928463	0.00137383	0.00237507
4	4	−0.000398232	−0.00276132	0.00115615

lar momentum (already recognized by Vokrouhlický et al. (2007)). In particular, stable spiral points appear in SAM+ and LAM–, having increasing G, while unstable spiral points that emerge in SAM– and LAM+ are associated with decreasing G value. Both types are related to $\theta \approx 45^\circ$, and ε trapped around 55° or 125°. The SAM– state is generally unstable – all the orbits leave it through the separatrix. Moreover, the previously undetected limit cycles in LAM were observed: stable (LAM+) and unstable (LAM–). All the trajectories originating inside them stay in the LAM. The rotation around the principal axis appears to be unstable under the action of YORP torque; the tumbling motion tends to be sustained. With the loss of angular momentum and rotation rate, the chaotic zone around separatrices expands, eventually destabilizing the asymptotic points or cycles.

How does the picture change after including the inelastic dissipation? The results of our simulations are displayed as curves in the plane of θ and $\xi = \cos\varepsilon$, originating at cross marks. The grey area covers the values of nutation angle below 15° that are not recognizable as NPA rotation with the use od standard photometry (Henych & Pravec 2013). Generally, in (θ,ξ) plane, inelastic dissipation acts by pushing the plot points horizontally to the left; any vertical motion is exclusively YORP-driven, and any motion to the right means that the YORP effect overpowers the inelastic dissipation. During the evolution of rotation state, the strength of inelastic dissipation is affected by two factors: it decreases when approaching the principal axis (small θ) or when the rotation slows down (crossing the areas where $\dot{G} < 0$ due to the YORP).

Fig. 2 presents the evolution of Eger in SAM. In SAM+, presented in left panel, there are three possible final states. If evolution starts at $|\xi| \gtrsim 0.8$ (almost normal to the orbital plane), the wobbling is damped to principal axis rotation. The curves starting at smaller $|\xi|$ are initially are driven leftwards, but once the dissipation weakens at $\theta < 20^\circ$, they are repelled from the principal axis region by the YORP. Some of them ($|\xi| = \cos 40^\circ \approx 0.77$) hit the separatrix, and their future fate is unknown. The same initial conditions for the YORP alone, would bring the motion towards one of the stable spiral points at $\xi \approx 0.6$, known from Fig. 4 (SP) of Breiter et al. (2011), but the dissipation destroys the attractors. However, some other interesting feature appears: the curves originating closer to the value of $\varepsilon = 90^\circ$ reach a stable state of tumbling in the orbital plane with constant period of around 10 h and nutation angle $\sim 47^\circ$. This third final state is a real novelty.

When discussing the YORP effect, one may notice that the difference between SAM+ and SAM– amounts to a simple time reversal, leaving the shape of the curves intact. But there, the integral curves on the (θ,ξ) plane did not depend on the value of angular momentum G. Now the situation is quite different, and the interchanging of the positive and negative $\dot{G}$ areas has serious consequences. The orbits with $60^\circ \lesssim \varepsilon \lesssim 120^\circ$ (i.e. $|\xi| \lesssim 0.5$) end up at the principal axis, whereas those further from the orbital plane are dragged back to the right and then drift towards the former unstable spiral point from Fig. 4 (SM) of Breiter et al. (2011). We cannot exclude a further migration to $\xi = 0$, like it has happened in SAM+, but the drift takes place in the $\dot{G} < 0$ area, so we stop the integration at the rotation period of 10 years, considering further tracking unreasonable.

In addition, we performed the integration for the mirror Eger shape introduced in (Breiter et al. 2011), that is, the shape of Eger as reflected with respect to the xz plane; the results are similar to the ones for ordinary Eger with reversed +/– mode sign.

The long axis mode with the YORP alone presented a rich portrait with spiral points and stable limit cycles. None of them survives the presence of inelastic dissipation and all the trajectories we tested exited this mode through the separatrix. This should be expected, because energy dissipation in LAM is considerably stronger than in SAM (Breiter et al. 2012).

Scaling Eger down by factor 10, we have obtained an example of a hundred-meter size body. Appropriate adjustments include multiplying the moments of inertia by 10^{-5}, and the volume by 10^{-3}. As it follows from Eq. (3), the energy dissipation is much weaker for such a body, whereas the YORP effect is stronger. Indeed, Fig. 3 is much more YORP-like; it does resemble Fig. 4 of Breiter et al. (2011), yet with one notable exception. In the pure YORP case, the stable spiral point in SAM+ corresponds to the growth of angular momentum. But this increases the energy dissipation and after 22 My, the angular momentum vector is brought to the equilibrium in the orbital plane – the same as in Fig. 2, but with a 10 times shorter rotation period of 1 h. In SAM–, trajectories quickly end up in the vicinity of the separatrix, in good agreement with the YORP-only evolution.

The LAM rotation (Fig. 4) progresses almost similarly to the pure YORP case, but the stable limit cycles are no longer present and sooner or later, all the trajectories leave the mode. Most of those entering through the separatrix do it rather quickly. In LAM+, the curves coming from the inside of the previous limit cycle and the ones attracted to it from the outside, slide along its remnants but they are forced by inelastic dissipation to finally hit the separatrix. In LAM–, the attracting equilibrium points coincide with $\dot{G} > 0$, so the angular momentum can stay there only until the increasing energy dissipation rate removes it into the separatrix zone.

Increasing the size of Eger 10 times, we have obtained a quick migration to the principal axis rotation with no observable distortion of paths due to the YORP.

4.2 (99942) Apophis

Due to its moderately excited state, the rotation of (99942) Apophis must be shaped by the influence of both YORP effect and inelastic energy dissipation. Since only the latter has been addressed by Pravec et al. (2014), we begin by studying the influence of the YORP alone for various possible initial rotation states of this object. Figure 5 shows the results obtained in SAM and LAM. Only the SAM+ and LAM+ are displayed, because, as already noted, the curves for SAM– and LAM– look similarly, except that they are traversed in the opposite direction.

Although lacking stable limit cycles, Fig. 5 remains similar to the case of Eger by the presence of equilibria at $\theta \approx 25^\circ$, $\varepsilon \approx 37^\circ, 143^\circ$ (SAM) or $\theta \approx 38^\circ$, $\varepsilon \approx 55^\circ, 125^\circ$ (LAM). In SAM+, the spiral points are unstable and placed at the $\dot{G} < 0$ area; and

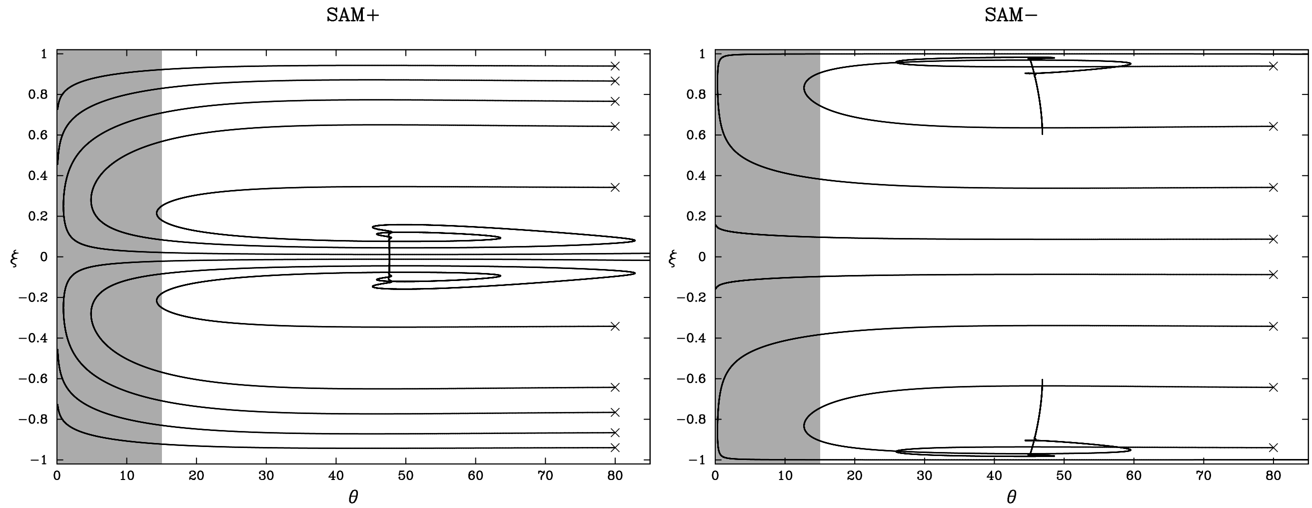

Figure 2. Evolution of the Eger rotation in SAM, projected on the plane of nutation angle θ (in degrees) and cosine of obliquity ξ.

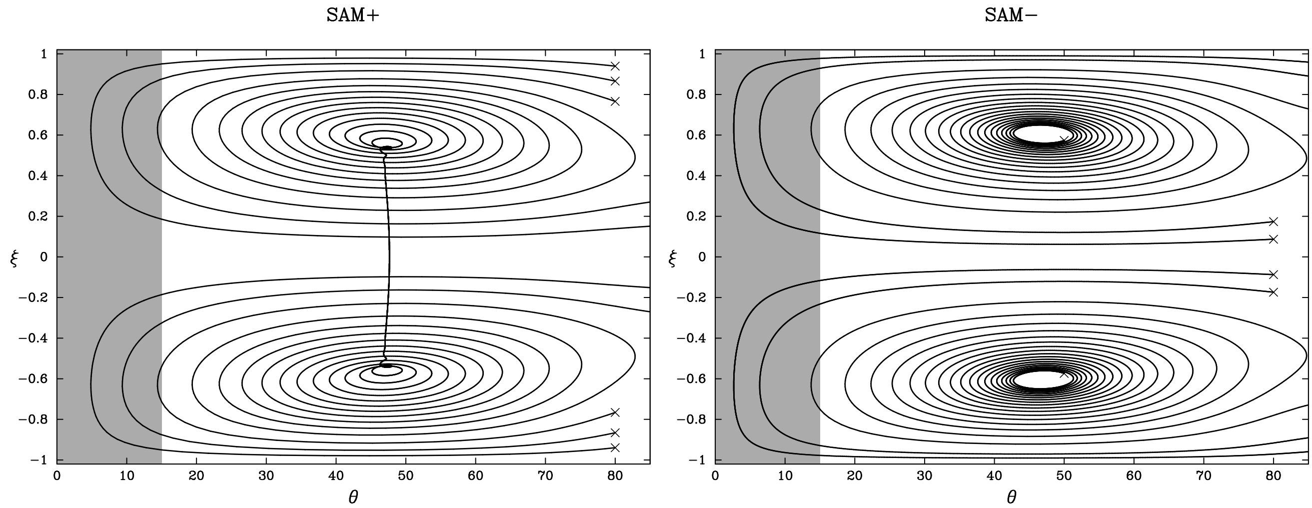

Figure 3. Evolution of rotation for a 10 times smaller Eger shaped object.

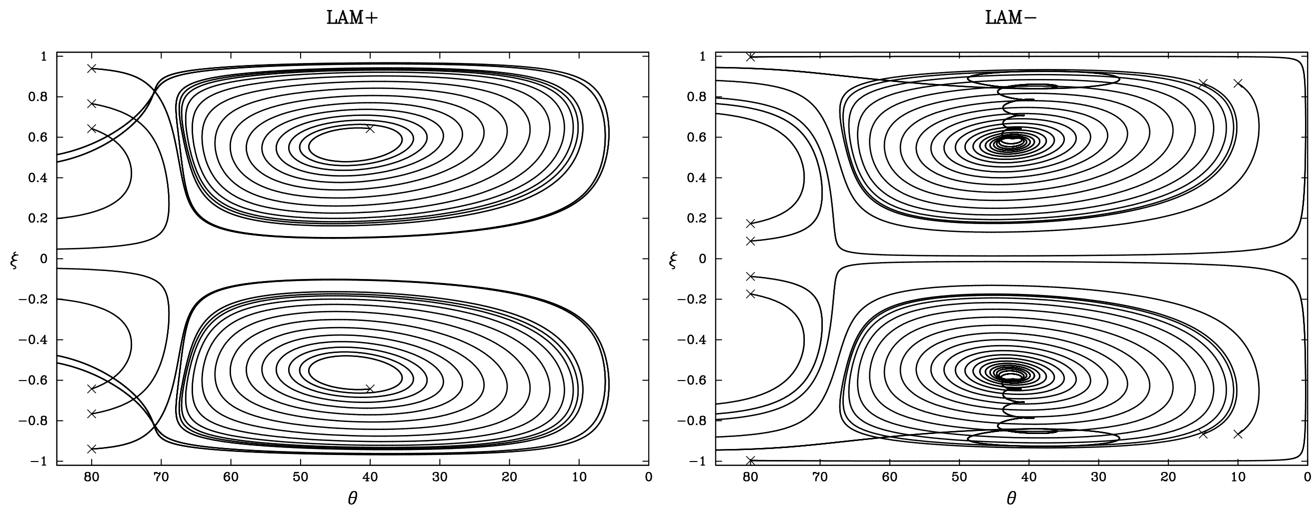

Figure 4. Same as in Fig. 3 but for the LAM case.

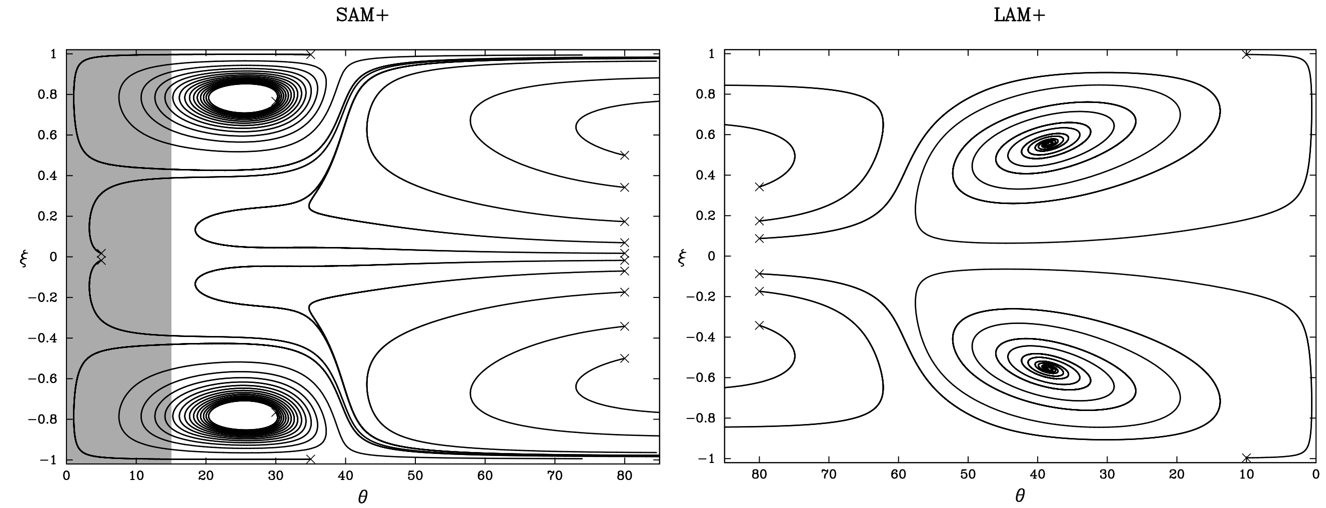

Figure 5. Evolution of (99942) Apophis rotation under the action of the YORP effect alone.

SAM– is opposite in both respects. The spiral points of LAM+ are stable, having a larger basin of attraction than their short axis mode analogues. Their location corresponds to the speed-up of rotation ($\dot{G} > 0$) which would imply a stronger stability as far as the YORP is concerned, but it makes them vulnerable to the inelastic energy dissipation. Generally, from the point of view of the YORP effect, Apophis has no chance to exhibit a regular rotation and either should settle down in one of the LAM+ or SAM– stationary tumbling states, awaiting a fission breakup, or – more likely – it should irregularly revisit the chaotic separatrix neighborhood.

Fig. 6 displays how the evolution of both SAM types of rotation is altered when energy dissipation is taken into account. The trajectories in SAM+ seem to be only slightly disturbed. Obviously, the most interesting is the actually observed rotation state of Apophis. The initial conditions from Pravec et al. (2014) are marked with a red star. They refer to $\theta = 55^\circ$, although the error bounds imply $35^\circ < \theta < 64^\circ$. However, any value in this range leads Apohis towards the separatrix (in less than 2 ky for the nominal red curve originating at $\theta = 55^\circ$). On the other hand, even smaller error bounds would not allow to distinguish if the present state has been reached from the separatrix zone, or from the neighborhood of the principal axis. A positive statement can be made, that the majority of the initial states with retrograde rotation are YORP-driven close to $\varepsilon = 180^\circ$, so the present obliquity of Apophis does not contradict the model and may be considered natural. Interestingly, the action of the YORP in the principal axis rotation would be quite different, driving the spin axis towards $\xi \approx 0.4$.

The spiral points in SAM– are only temporarily stable after the addition of nutation damping; while nutation angle θ and period P reach asymptotic values of approximately 25° and 1.2 h, respectively, the obliquity of angular momentum slowly slides towards 0° or 180°, where the stable point is found after over 600 My. Assuming the Apophis to be in the SAM– rotation (which means $\theta = 55^\circ$ measured from the south pole of the shape model) we see that in 3 My its tumbling should be damped, resulting in the principal axis rotation, with $\varepsilon = 90^\circ$, and a systematic speed-up. Yet, thinking about error bounds on θ, any other scenario is likely. On the other hand, the past is fixed, implying the arrival from the separatrix zone, although with rather particular obliquity, close to its present value.

The situation in LAM, shown in Fig. 7, resembles the SAM case: the curves are only slightly distorted by the inelastic energy dissipation and only the behaviour of the previously stable spiral points in LAM+ is different. Growing angular momentum increases energy dissipation, and the latter results in the drift towards the separatrix. All trajectories originating in LAM– exit this mode through separatrix similarly to the proper YORP case.

Increasing the diameter of Apophis by the factor of 10, we obtain an object comparable in size to the actual Eger. We have studied the scaled asteroid in all rotation modes, but only the short axis mode (Fig. 8) reveals new features. A SAM+ pair with initial $\varepsilon = 80^\circ, 100^\circ$ (i.e. $|\xi| \approx 0.17$) was attracted by the YORP-unstable spiral points ($\theta \approx 25^\circ$ and $\varepsilon \approx 38^\circ, 142^\circ$), where it stayed until the rotational period exceeded the assumed limit of 10 y. Another SAM+ pair, starting at $\varepsilon = 85^\circ, 95^\circ$ (i.e. $|\xi| \approx 0.09$) also migrates towards the same spiral points but spends a considerable time looping around them until it spirals outward to hit the separatrix. In SAM– (Fig. 8 right), the majority of trajectories entering through the separatrix leave this mode. However, those with initial obliquity close to 0° or 180° are attracted by the former sink at $\theta \approx 25^\circ$, where the rotation period stabilizes close to 12 h. Like in Fig. 6, the obliquity is asymptotically driven towards 0° or 180°, but the process is 10 times longer. Although the object is hypothetic, we have retained the red star for the initial conditions of the actual Apophis or its SAM– version.

5 FINAL STATE MAPS

In previous Sections we have identified 4 basic outcomes of simulation for the two exemplary objects. In order to acquire some idea about how likely is each of them, we performed six scans on grids of 629 initial conditions of nutation angle $2^\circ \leqslant \theta \leqslant 82^\circ$, and obliquity $0^\circ \leqslant \varepsilon \leqslant 180^\circ$, with a 5° spacing in both variables. The results are presented in Fig. 9, where the shade of each rectangle represents the final state resulting from the initial conditions located at its centre. White colour refers to entering a potentially chaotic zone around a separatrix. Light grey means that the rotation period decreased to the level of 10 y – an unstable state beyond the limits of validity for the model. Dark grey indicates a stationary tumbling with an asymptotically fixed rotation period. Finally, the principal axis rotation is marked black. All initial conditions for a given ob-

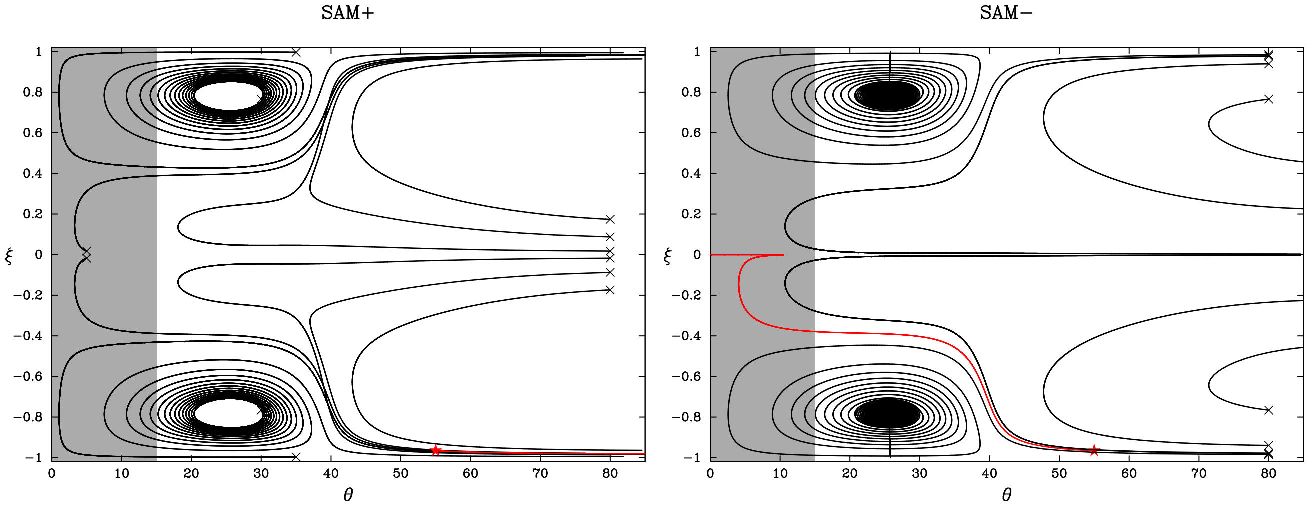

Figure 6. Evolution of SAM rotation under the action of YORP effect and inelastic energy dissipation for (99942) Apophis.

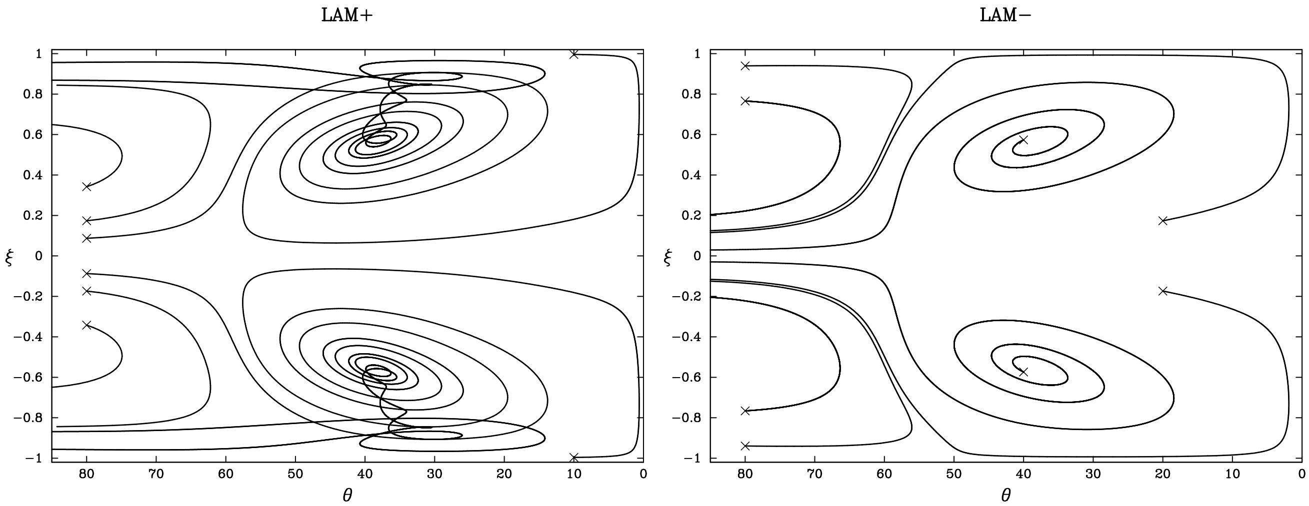

Figure 7. Same as in Fig. 6 but for LAM rotation.

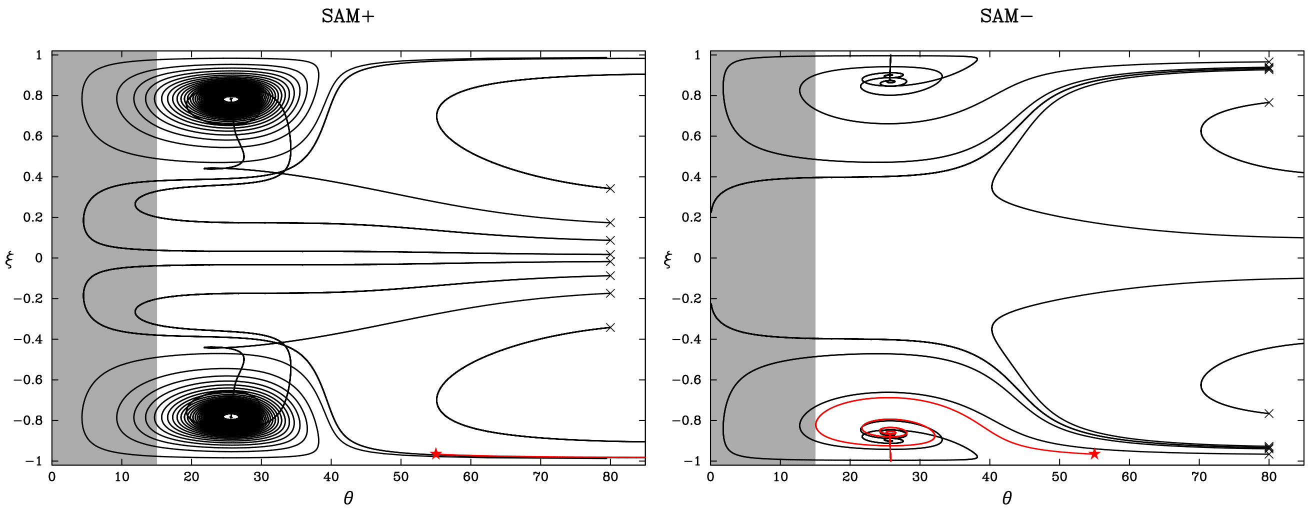

Figure 8. Rotational evolution of 10 times larger Apophis in the case of SAM.

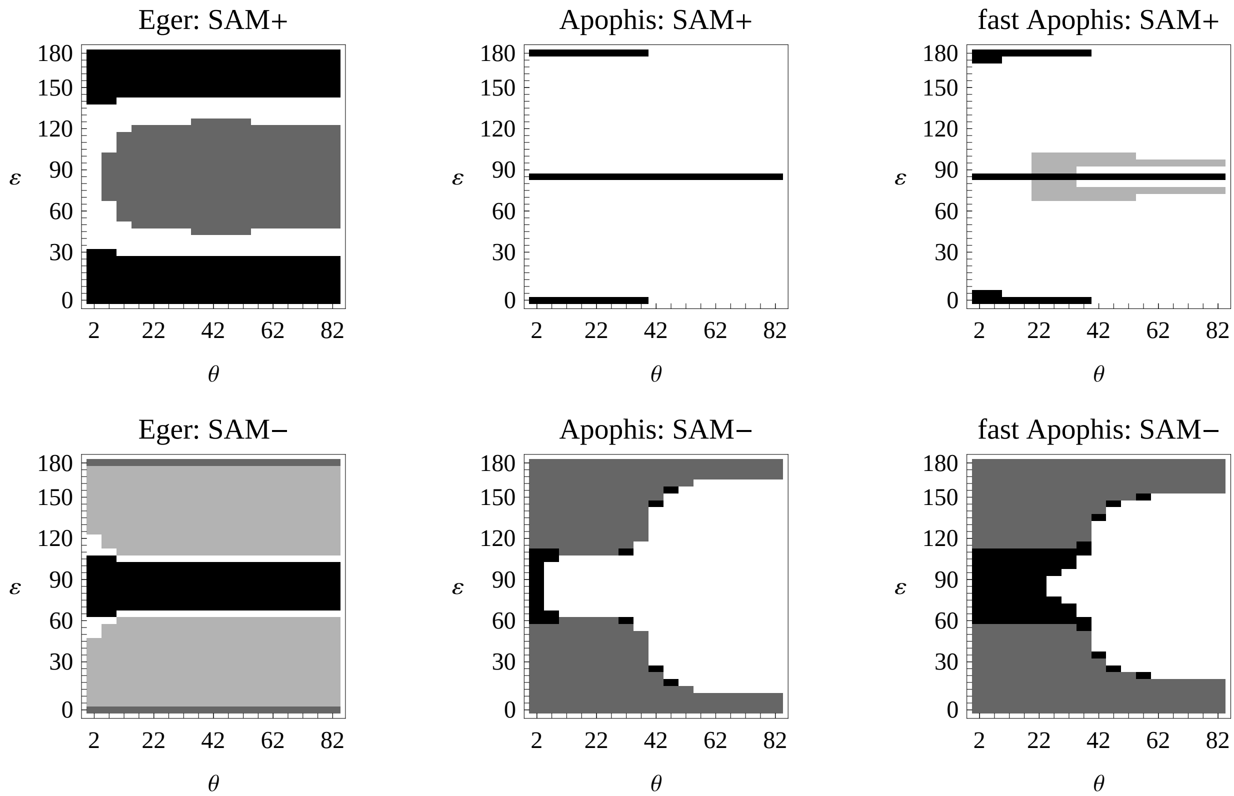

Figure 9. Final states reached from given initial conditions ($5^\circ \times 5^\circ$ grid) in SAM mode for Eger (left), Apophis (middle) and a 10 times faster spinning Apophis shaped body (right). Shades legend: white – separatrix zone, light grey – period decreased below 10 y, dark grey – stationary tumbling with stable period, black – principal axis rotation.

ject use the same rotation period P, and the damping parameter was set $\mu Q = 10^{11}$Pa.

For an Eger-shaped body (P = 5.7 h) in SAM+, a moderate fraction of initial states (38%) results in the actually observed principal axis rotation. In SAM– the fraction is smaller, i.e. about 20%. In both cases the basin of attraction for the principal axis rotation is well confined for the obliquity: 30° around the orbit normal in SAM+, and ±30° around the orbital plane in SAM–. Since the actual rotation state of Eger is $\theta < 15^\circ$, and $\varepsilon \approx 175^\circ$ (SAM+), there is no contradiction between the adopted model and observational facts. Interestingly, the majority (69%) of the initial conditions in SAM– leads to the critical slowdown to $P > 10$ h, making the tumbling around the south pole of the Eger figure model quite unlikely – even more if we add the 6% for the separatrix zone hits. The situation in SAM+ is different, because only 24% of the cases exit this mode through the separatrix, whereas the remaining 38% settles in down in stationary tumbling. The last state emerged also in SAM– in 5% of the cases, but it happened only for the angular momentum normal to the orbital plane. From the point of view of the statistics provided by Pravec et al. (2014, Fig. 8), the dimension and rotation period of Eger locate it in the area completely dominated by principal axis rotators. In these circumstances, the 29% of initial conditions leading to this state from both SAM modes is rather less that expected.

The Apophis, less affected by the inelastic dissipation due to its smaller radius and a longer rotation period (P = 30.5 h), has a different statistics of the final states (Fig. 9 – middle). The SAM+ is mostly unstable: 95% of initial conditions end up in the separatrix zone. The remaining 5% lead to the principal axis rotation – all concentrated in particular lines of $\varepsilon = 0^\circ, 90^\circ, 180^\circ$. Indeed, one might guess this result from the small sample shown in Fig. 6. The situation in SAM– is more interesting: although 52% of cases lead to the separatix, and only 3% end in the principal axis, a significant remainder of 44% results in stationary tumbling. In contrast to the SAM+, the principal axis rotation results from initial conditions on the border between well separated separatrix and stationary tumbling zones. It seems that according to the present model, an Apophis precessing around the south pole of its figure model would be more likely than the actually observed one unless, apart from the limitations of the model, its present rotation state is relatively young (less than $\sim 10^3$ y since a collision or since the exit from the separatrix zone). Overall, the simulation is coherent with the placement of Apophis in tumbling rotation zone of Pravec et al. (2014, Fig. 8).

In order to estimate the influence of the initial rotation period on the distribution of the final states, we have increased the rotation rate of an Apophis-shaped body. The "fast Apophis" considered in Fig. 9 (right) has a ten times shorter initial period P = 3 h. The difference is not drastic. In SAM+, a small area of critical slow-down ($P < 10$ y) has appeared, involving 7% of the initial states – all in the neighborhood of the orbital plane. The small (6%) fraction of the the initial conditions ending in the principal axis are mostly placed along $\varepsilon = 90^\circ$, and at the normal to the orbital plane. Nevertheless, the overwhelming majority (87%) lead to the separatrix.

The patterns in SAM– remain similar, although proportions have changed in favor of principal axis (13%), and stationary tumbling (49%). However, still 39% of initial conditions lead to the separatrix. Thus, principal axis rotation is unlikely for the "fast Apophis", yet it should be placed in the region dominated by principal axis rotators according to Pravec et al. (2014, Fig. 8).

6 CONCLUSIONS

Aware of all handicaps and limitations of the applied model, we hope that some patterns revealed in the present study may have reference to physical reality. In our opinion, the most interesting result is the existence of stationary tumbling states as attractors in the discussed model. Unlike the pure YORP states, they involve a stabilized rotation period on a physically plausible limit of few hours. The nature of these states is definitely worth further investigation. For a while, we can only remark, that their location and presence is determined by two factors: first, it must coincide with a $\dot{G} = 0$ line which is exclusively YORP-based; second, it needs an equilibrium between the opposite action of inelastic dissipation and the YORP in nutation angle θ. Physical properties of an asteroid don't have much influence on the former, but the latter is strongly dependent on both damping coefficient μQ and thermal conductivity. Regretfully, the influence of the thermal conductivity in the tumbling rotation YORP is yet a domain of speculations. One may guess it to be analogous with the YORP in obliquity for the principal axis rotation, i.e. decreasing the strength by a constant factor if the conductivity is small. If the guess is true, the stationary tumbling should happen closer to the principal axis – maybe even in the $\theta \lesssim 15^\circ$ zone observationally considered a simple rotation state. Depending on the values of the YORP-induced $\dot{\varepsilon}$, the tumbling state may either become stationary at some arbitrary ε, or it slides along a $\dot{G} = 0$ curve to $\varepsilon = 0^\circ$, 90°, or 180° – all the three values having $\dot{\varepsilon} = 0$ (true only in linear thermal models or in a circular orbit case – see Breiter et al. (2010)). It is also not clear, to what extent the situation will change if a more elaborate rheology model replaces the constant μQ parameter.

The above remarks about the dependence on physical parameters remain of importance when we try to judge the present model in the context of prevailing principal rotation states in the observational data. The fraction of principal rotation states resulting from our simulations is definitely too low to match reality. Moreover, it may even be overestimated due to stopping the integration at $\theta = 0.^\circ1$, which gives no chance to a long-term, YORP-based destabilization. Thus, a reasonable conclusion is that either the energy dissipation mechanism should be considerably stronger than assumed, or the action of YORP in the spin axis attitude should be weaker, or – most likely – both.

ACKNOWLEDGEMENTS

The authors thank Michael Efroimsky, Petr Pravec, and David Vokrouhlický for their comments and help in providing some data and references.

REFERENCES

Breiter S., Bartczak P., Czekaj M., Oczujda B., Vokrouhlický D., 2009, A&A, 507, 1073
Breiter S., Bartczak P., Czekaj M., 2010, MNRAS, 408, 1576
Breiter S., Rożek A., Vokrouhlický D., 2011, MNRAS, 417, 2478
Breiter S., Rożek A., Vokrouhlický D., 2012, MNRAS, 427, 755
Burns J. A., Safronov V. S., 1973, MNRAS, 165, 403
Čapek D., Vokrouhlický D., 2004, Icarus, 172, 526
Cicaló S., Scheeres D. J., 2010, Celest. Mech. Dyn. Astron., 106, 301
Efroimsky M., 2000, J. Math. Phys., 41, 1854
Efroimsky M., Makarov V. V., 2013, ApJ, 764, 26
Everhart E., 1985, in A. Carusi, G.B. Valsecchi, eds, IAU Colloq. 83: Dynamics of Comets: Their Origin and Evolution. D. Reidel Publishing Company, p. 185
Golubov O., Krugly Y. N., 2012, ApJL, 752, L11
Henych T., Pravec P., 2013, MNRAS, 432, 1623
Müller T. G., Kiss C., Scheirich P., Pravec P., O'Rourke L., Vilenius E., Altieri B., 2014, A&A, 566, A22
Pravec P. et al, 2014, Icarus, 233, 48
Prendergast K. H., 1958, AJ, 63, 412
Rubincam D. P., 2000, Icarus, 148, 2
Sharma I., Burns J. A., Hui C.-Y., 2005, MNRAS, 359, 79
Statler T. S., 2009, Icarus, 202, 502
Vokrouhlický D., Breiter S., Nesvorný D., Bottke W. F., 2007, Icarus, 191, 636
Wiegert P. A., 2015, Icarus, 252, 22